Macromolecular Bioscience
www.mbs-journal.de

Polyoxazolines with Cholesterol Lipid Anchor for Fast Intracellular Delivery

Laurianne Simon, Liên Sabrina Reichel, Belkacem Tarek Benkhaled, Jean-Marie Devoisselle, Sylvain Catrouillet, Juliane Eberhardt, Stephanie Hoeppener, Ulrich S. Schubert, Johannes Christopher Brendel, Marie Morille, Vincent Lapinte, and Anja Traeger**

Due to the increasing challenges posed by the growing immunity to poly(ethylene glycol) (PEG), there is growing interest in innovative polymer-based materials as viable alternatives. In this study, the advantages of lipids and polymers are combined to allow efficient and rapid cytoplasmic drug delivery. Specifically, poly(2-methyl-2-oxazoline) is modified with a cholesteryl hemisuccinate group as a lipid anchor (CHEMSPOx). The CHEMSPOx is additionally functionalized with a coumarin group (CHEMSPOx-coumarin). Both polymers self-assembled in water into vesicles of ≈100 nm and are successfully loaded with a hydrophobic model drug. The loaded vesicles reveal high cellular internalization across variant cell lines within 1 h at 37 °C as well as 4 °C, albeit to a lesser extent. A kinetic study confirms the fast internalization within 5 min after the sample's addition. Therefore, different internalization pathways are involved, e.g., active uptake but also nonenergy dependent mechanisms. CHEMSPOx and CHEMSPOx-coumarin further demonstrate excellent cyto-, hemo-, and membrane compatibility, as well as a membrane-protecting effect, which underlines their good safety profile for potential biological intravenous application. Overall, CHEMSPOx, as a lipopolyoxazoline, holds great potential for versatile biological applications such as fast and direct intracellular delivery or cellular lysis protection.

1. Introduction

Polymeric particles have been extensively used in nanomedicine for cellular delivery of active molecules e.g., for cancer therapy.[1] They can be composed of amphiphilic polymers, which are able to self-assemble in aqueous media and to create nanosized objects with a hydrophobic core and a hydrophilic shell. The amphiphilic character of the polymeric nanocarriers enables loading and protection of the active molecules, especially hydrophobic drugs, and leads to enhanced cellular uptake and drug retention in tissues.[2] Among synthetic amphiphilic polymers, diblock copolymers (e.g., hydrophobic poly(styrene) or poly(caprolactone)s associated with hydrophilic poly(ethylene glycol)s) and triblock (e.g., poloxamers) are often employed for such purposes.[2] A controlled synthesis with a defined monomer composition, degree of polymerization, molar mass, structural configuration (e.g., diblock and triblock), and morphology (e.g., linear, stellate, and dendritic), in conjunction with the introduction of functional groups, enables a nanocarrier design with specific properties such as surface

L. Simon, B. T. Benkhaled, J.-M. Devoisselle, S. Catrouillet, M. Morille, V. Lapinte
ICGM
CNRS
ENSCM
Univ. Montpellier
Montpellier, France
E-mail: vincent.lapinte@umontpellier.fr

L. S. Reichel, J. Eberhardt, S. Hoeppener, U. S. Schubert, J. C. Brendel, A. Traeger
Laboratory of Organic and Macromolecular Chemistry (IOMC)
Friedrich Schiller University Jena
Humboldtstrasse 10, 07743 Jena, Germany
E-mail: anja.traeger@uni-jena.de

S. Hoeppener, U. S. Schubert, J. C. Brendel, A. Traeger
Jena Center for Soft Matter
Friedrich Schiller University Jena
Philosophenweg 7, 07743 Jena, Germany

M. Morille
Institut universitaire de France (IUF)
Paris, France

The ORCID identification number(s) for the author(s) of this article can be found under https://doi.org/10.1002/mabi.202400148

DOI: 10.1002/mabi.202400148

charge, stability, and drug encapsulation capacity.[3] This careful orchestration allows the properties of nanocarriers to be tailored in a defined manner.

The most common hydrophilic polymer for micellar drug delivery is poly(ethylene glycol) (PEG). It is known to induce steric stabilization and stealth behavior.[4] However, its systematic use has led to an increased number of people worldwide with anti-PEG antibodies.[4–7] This issue has been intensified with the use of PEGylated mRNA vaccination.[8–10] In addition, PEGylation can lead to reduced cellular internalization and endosomal escape of polymeric micelles due to the steric hindrance of the PEG corona, known as the PEG dilemma.[11] Thus, alternatives to the use of PEG need to be found and poly(amino acid)s, poly(acrylamide)s, or poly(oxazoline)s are among the potential candidates.[4,12] The poly(oxazoline) family, also called POx, has sparked great interest as a polymer alternative drug delivery system, hydrogels, or biomaterials over the last few years.[13–16] Indeed, POx gathers interesting biological properties, such as cyto- and hemocompatibility, immunomodulation, and stealth behavior.[16] The latter is due to tight associations of the hydrophilic polymer around nanoparticles with the hydrating layer. In addition, cationic ring-opening polymerization provides control over the end groups, molar mass, and the distribution of POx.[17] Furthermore, a wide range of variations in the monomer side groups and polymer architectures enable access to responsive or smart materials.[15,18,19]

Lipopoly(oxazoline)s, also called LipoPOx, is an amphiphilic POx modification with 2-methyl-2-oxazoline-based polymers as a hydrophilic element and a lipid chain as a hydrophobic moiety.[20] Due to their amphiphilic nature, lipid polymers can also assemble into polymeric vesicles or micelles.[21] Such LipoPOx, were synthesized with various possible lipid anchors such as with phospholipid anchors (distearoylphosphatidylethanolamine),[22] or linear structures (saturated C_{16} and unsaturated $C_{18:2}$) or grafted ones (with $C_{18}(SC_{12})_2$ and $C_{18}(SC_8)_2$).[23] LipoPOx were also able to form stable drug delivery systems such as liposomes.[23] Above all, the lipid anchor was shown to interact and insert in the lipid membrane as confirmed for giant unilamellar vesicles (GUV), cell membranes, and skin.[24] The kinetic of insertion was found to be different depending on the nature of the lipid anchor. For example, in contrast to the linear unsaturated $C_{18:2}$, the linear saturated C_{16} was able to be inserted in GUV and cell membranes immediately after addition.[24]

Looking for other lipid anchors with rapid membrane insertion ability, cholesterol, and phospholipids derivatives are often used for this purpose. However, the net anionic charge on the phosphate moiety of phospholipid-PEG derivatives was reported to play a key role in complement activation.[25] Thus, cholesterol anchors in regard to their low cost, stability, and ease of handling emerged as the most suitable option compared to phospholipids. Moreover, cholesterol is known to be an essential component of the cellular membrane and plays a significant role in modulating its structural (fluidity and permeability) and dynamic properties.[26] Therefore, cholesterol has already been grafted to polymers to benefit from these properties for enhanced cellular internalization.[27,28] A majority of the studies used cholesteryl anchors conjugated with the "gold standard" PEG[29] to be associated with liposomes or lipid nanoparticles for establishing stealth behavior and improved drug delivery.[26] Poly(2-ethyl-2-oxazoline) functionalized cholesterol has also been investigated to be inserted in liposomes.[30,31] However, to the best of our knowledge, the application potential of the highly amphiphilic cholesterol-poly(2-methyl-2-oxazoline) has not been studied in the form of a polymeric micelle without further additional components.

To investigate the potential of this stealth lipid, a cholesteryl hemisuccinate group (CHEMS) as lipid anchor was grafted onto poly(2-methyl-2-oxazoline) using a cleavable linker (CHEMSPOx). In addition, **CHEMSPOx** was functionalized with a coumarin group (**CHEMSPOx-coumarin**) using a coumarin-functionalized initiator for the first time. Coumarin is known as an active molecule and for the ability to dimerize under UV light and fluorescent signal.[32,33] The obtained self-assembly structures of **CHEMSPOx**, **CHEMSPOx-coumarin**, and their loaded version with the hydrophobic fluorescent neutral lipid orange dye (NLO) were investigated in terms of size, structure, as well as physicochemical and biological performance e.g., cellular interaction, membrane fusion, and membrane protective effect.

2. Results and Discussion

2.1. Synthesis of CHEMSPOx

This study investigated the potential for intracellular delivery of polyoxazolines with 2-methyl-2-oxazoline monomer-bearing cholesteryl group called **CHEMSPOx**. **CHEMSPOx** was reported for the first time utilizing 2-ethyl-2-oxazoline monomer as an unfunctional initiator like MeOTs[30] but has never been synthesized using coumarin-functionalized initiators. The terminal functionalization of POx by coumarin derivatives has been previously described using an initiator bearing a C_{11} chain alkyl spacer between the tosylate and coumarin functions.[34] In this study, the same strategy was performed (**Scheme 1**) but using a C_2 spacer to limit the impact of the coumarin addition on **CHEMSPOx** behavior and to maintain the balance between hydrophilicity and lipophilicity. The synthesis of both **CHEMSPOx** and **CHEMSPOx-coumarin** was conducted similarly using MeOTs or Coum-ethyl-OTs initiators respectively. In a second step, the POx(-coumarin) was ω-functionalized by a cholesteryl group (CHEMS) using a hemisuccinate cleavable linker.

The cationic ring-opening polymerization and the chemical post-modification were monitored by ^{1}H NMR spectroscopy as illustrated in **Figure 1** where characteristic signals of coumarin units were observed, such as aromatic protons in the region of 8–6 ppm as well as the methyl group at 2.4 ppm (H_{15}). Some isolated signals related to protons of cholesteryl unit were located at 5.3 ppm (H_5) or methyl groups at 0.6 (H_9) and 0.8 ppm ($H_{6,7}$) and allowed the calculation of a CHEMS functionalization of ≈90% (**Table 1**). For both initiators, the repetitive units per chain (DP_n) were close to 50 as shown in Table 1 (for CHEMSPOx: $DP_{n,exp} = 52$ vs $DP_{n,th} = 50$ and CHEMSPOx-coumarin: $DP_{n,exp} = 44$ vs $DP_{n,th} = 50$). In SEC chromatography, monomodal traces were observed with a dispersity (Đ) of 1.23 for **CHEMSPOx** and 1.33 for **CHEMSPOx-coumarin** (Figure S11, Supporting Information). This example of **CHEMSPOx-coumarin** highlights the possibility of easily ω-functionalize a POx tagged with a fluorescent coumarin moiety with any biologically active molecule functionalized with a hemisccinate group.

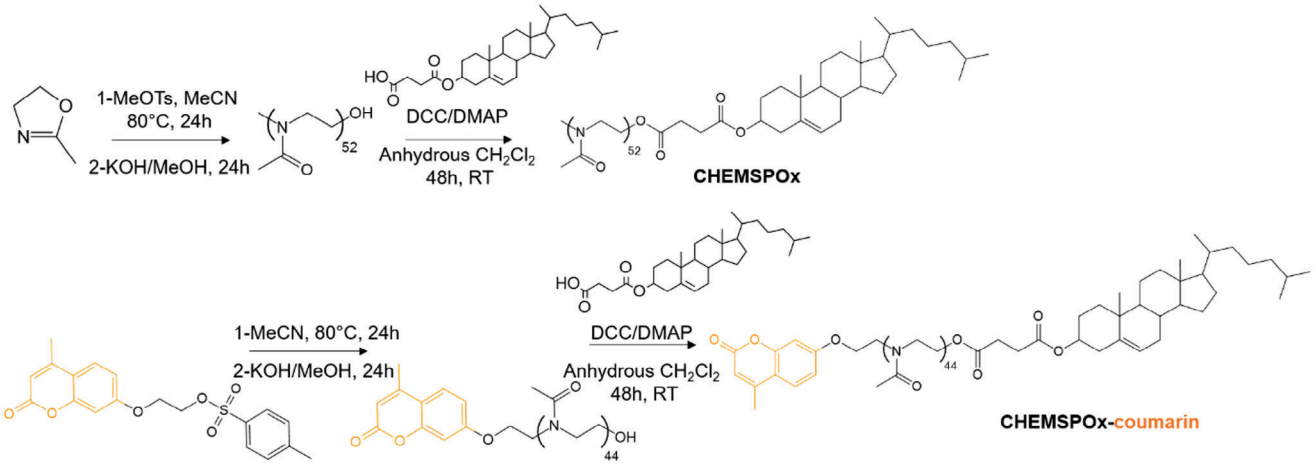

Scheme 1. Synthesis strategy of CHEMSPOx and CHEMSPOx-coumarin.

2.2. Characterization of CHEMSPOx Self-Assembly

Both polymers were dissolved in water at 2.5 g L^{-1} and incubated for 24 h with continuous stirring to allow complete solubilization. Due to the amphiphilic character of the polymer, nanosized vesicles can self-assemble as illustrated in **Figure 2A** and shown as DLS correlogram in Figure S12 (Supporting Information). A significant difference in the Z-average was observed with **CHEMSPOx** forming nano-assemblies of 120 ± 1 nm while **CHEMSPOx-coumarin** formed smaller assemblies at 98 ± 2 nm ($p < 0.001$) as shown in Figure 2B. Both samples had polydispersity indices (PDI) of 0.2 which indicates a homogeneous population and is common for polymer-based nanoparticles.[35] The CAC values were determined and revealed 190 ± 0.58 mg L^{-1} for **CHEMSPOx** and 162 ± 46.26 mg L^{-1} for **CHEMSPOx-coumarin** (Figure S13 and Table S3, Supporting Information). To further investigate the morphology of the obtained assemblies, cryoTEM imaging was performed (Figure 2C) and revealed the presence of multilamellar and unilamellar vesicles for both polymers with a large size distribution. A collection of cryoTEM images of **CHEMSPOx** vesicles is presented in Figure S14 (Supporting Information). To confirm the statistical nature of the observed shapes, a

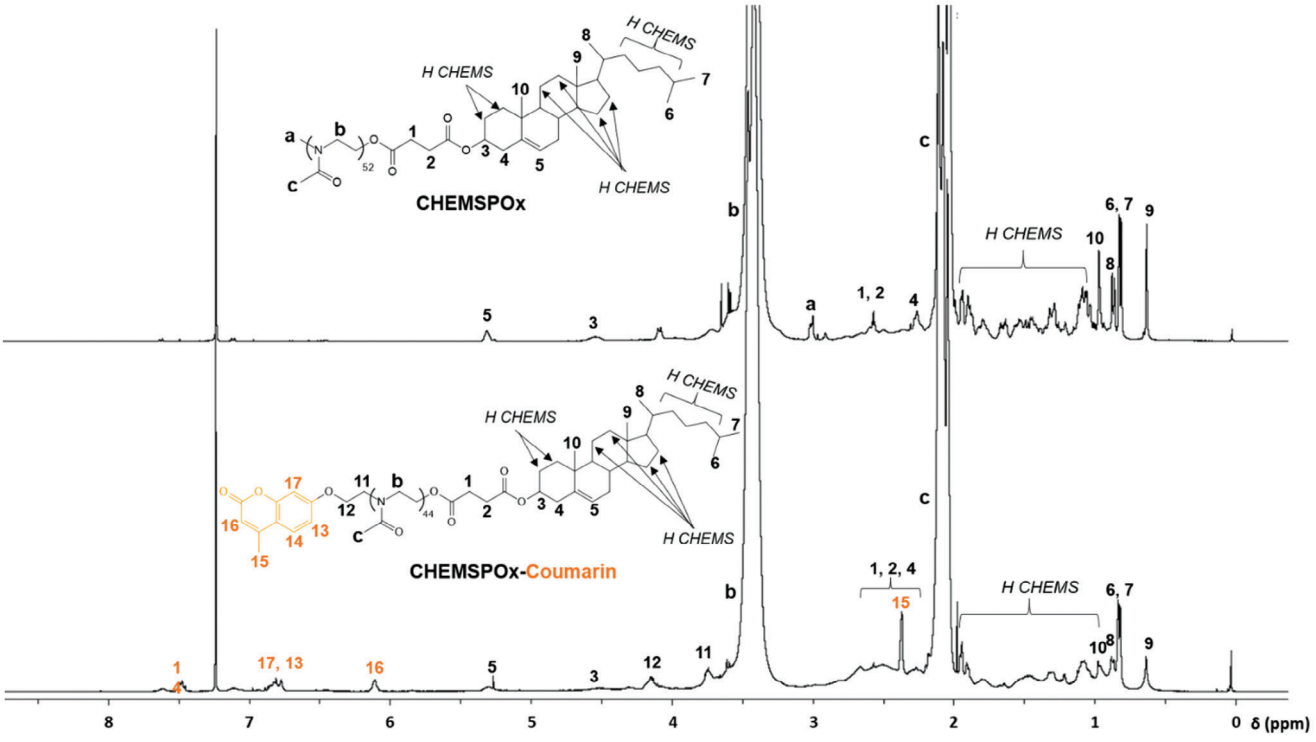

Figure 1. CHEMSPOx and CHEMSPOx-coumarin characterization with the ^{1}H NMR spectrum of the resulting polymers in $CDCl_3$.

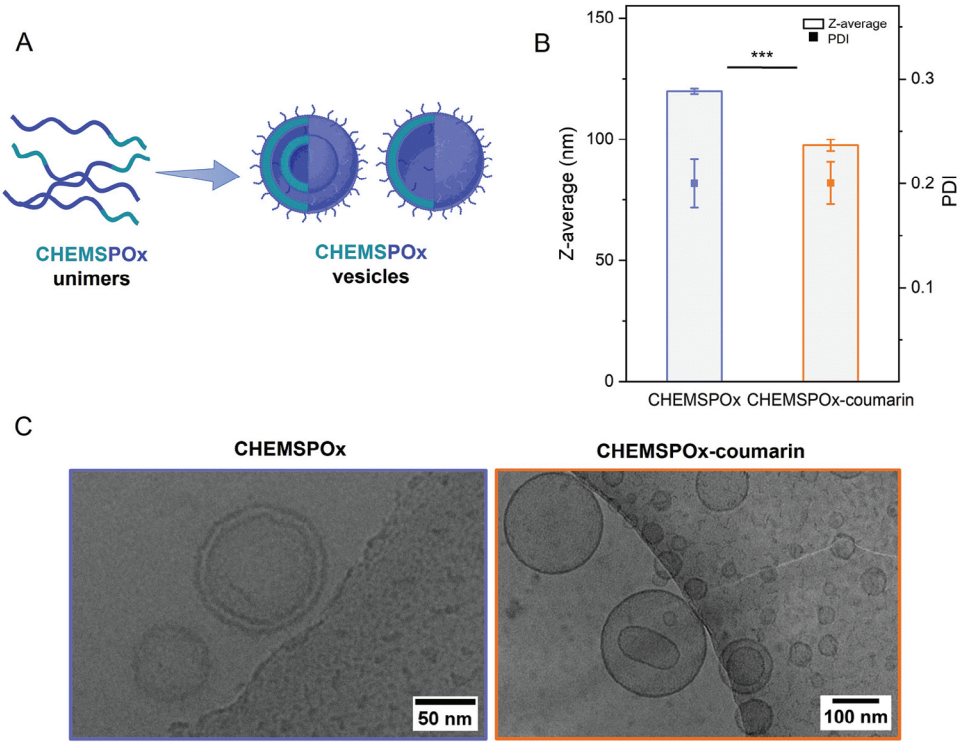

Figure 2. Characterization of **CHEMSPOx** (blue) and **CHEMSPOx-coumarin** (orange) self-assemblies with A) illustration of the obtained vesicles, B) size with Z-average (column) and PDI (dots) measured by DLS ($n = 3$, $^{***}p < 0.001$) and C) CryoTEM images of the formed structures in PBS.

static laser light scattering (SLS) study was conducted in addition to the cryoTEM observation (Figure S15, Supporting Information). The decrease of the intensity with q is due to the specific shape of the objects. Therefore, a form factor of a bilayered vesicle was used to fit the SLS data. An accurate fit was obtained with values of the internal radius and the thickness of the bilayer that matched the size observed in cryoTEM. The SLS data corroborate the cryoTEM observation albeit the absence of small q-range data does not fully validate these structures.

The obtained vesicles were stable upon dilution as illustrated by the NTA results (Figure S16, Supporting Information) with a dilution by a factor of 1000. A mean size of 107 nm with a calculated PDI of 0.11 for **CHEMSPOx** and 81 nm with a PDI of 0.15 for **CHEMSPOx-coumarin** was obtained, which underscores the DLS results. The thermodynamic stability of the formed **CHEMSPOx** and **CHEMSPOx-coumarin** vesicles at 4 °C was characterized via DLS at different storage time points over 17 months. The particle size of **CHEMSPOx** and **CHEMSPOx-coumarin** increased. More importantly, the PDI remained for both formulations below 0.3 over 17 months (Figure S17, Supporting Information).

Table 1. Summary of the CHEMSPOx and CHEMSPOx-coumarin characteristics.

Polymer	DP_n [a]	$M_{n\ NMR}$ [g mol^{-1}]	F_{CHEMS} [b] [%]	$F_{coumarin}$ [c] [%]
CHEMSPOx	52	4 900	87	/
CHEMSPOx-coumarin	44	4 450	91	100

[a] Value determined by ^{1}H NMR spectroscopy in $CDCl_3$ [b] F $\%_{CHEMS}$ = Functionalization rate of CHEMS [c] F $\%_{couamarin}$ = Functionalization rate of coumarin.

Alternative polyoxazolines bearing lipid anchors, such as, C_{16}POx, $C_{18:2}$POx, or $C_{18}(SC_{12})_2$POx formed 10 nm micelles[23] and those incorporating grafted POx within lipid chains (e.g., fatty ester and modified triglycerides) 10 to 20 nm micelles.[36] However, the cholesteryl anchor led to larger vesicles of 120 ± 1 nm. This led to the assumption that the variation in size and morphological structure is predominantly dictated by the lipidic block's rigidity. It is well known that amphiphilic copolymers self-assemble in solvents that are selective for only one of the building blocks and can thus generate different types of supramolecular assemblies such as micelles, worms, tubes, or vesicles depending on the composition, molecular weight, and relative length of the hydrophilic and hydrophobic moieties.[37] The **CHEMSPOx** with a small hydrophobic part and a large POx moiety led to the formation of conical shapes, a structure that is not supposed to spontaneously form vesicles, but rather micelles. Nevertheless, cryoTEM imaging evidenced a vesicular structure of **CHEMSPOx** self-assemblies. It should be stressed that it is the balance between all the free energy contributions to self-assembly and the kinetic factors that determine the morphology. The hydrophilic/hydrophobic ratio is an important factor, but never the only determining parameter. Our results confirm this tendency. Indeed, comparing with similar materials combining a cholesteryl group with other polymers, such as PEG, different sizes and shapes of self-assemblies were described. As an example, protoporphyrin IX conjugated with PEG_{2000} bearing two hydrophobic cholesteryl groups was dispersed in PBS and formed monodispersed micelles of 17 ± 3 nm

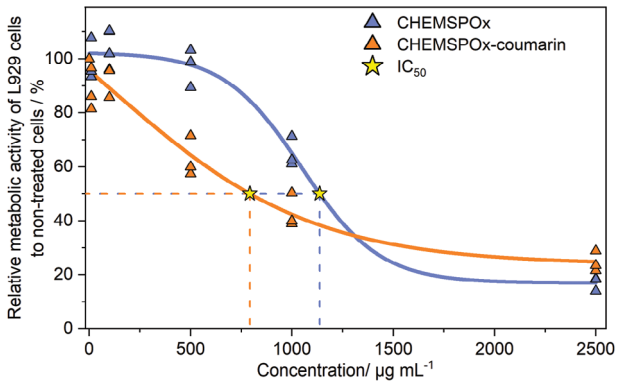

Figure 3. PrestoBlue assay was performed over 24 h in L929 cells. Dots represent values of single repetitions ($n = 3$), and lines represent the Dose-Response fit function. Stars indicate 50% toxic polymer concentration (IC_{50}).

(PDI of 0.13). However, no further investigation of their structure was performed.[38] To the best of our knowledge, **CHEMSPOx** is the first polymer ω-functionalized with a cholesteryl group, which can self-assemble into vesicles by simple dissolution in water. The incorporation of the coumarin did not modify the shape but decreased the size due to the addition of a hydrophobic group. Indeed, coumarin is a well-known photo-reactive chromophore with a fluorescence signal (λ_{Ex} 315 nm, λ_{Em}380 nm) as previously described.[34] Coumarin is able to dimerize into cyclobutane under UV illumination followed by a [2+2] cycloaddition as illustrated in Figure S18 (Supporting Information). The photo-dimerization of coumarin grafted on **CHEMSPOx** can be monitored by UV–vis spectroscopy. The UV absorption band decreased progressively until reaching a maximum of dimerization after 60 min of UV irradiation (Figure S18, Supporting Information). Furthermore, the fluorescence signal (λ_{Em} 380 nm) was maintained (Figure S19, Supporting Information) and was proportional to the concentration of **CHEMSPOx-coumarin** in PBS. In addition, the intrinsic UV properties of the coumarin group in **CHEMSPOx-coumarin** were analyzed and remained unchanged with grafting it onto the **CHEMSPOx**. These UV properties open up different perspectives of applications, such as the formulation of photo-active nanoparticles,[34] which can be used, for example, for photodynamic therapy.[39]

2.3. Investigation of Cellular Interactions

2.3.1. Cytotoxicity Study in L929 Cells (PrestoBlue Assay)

One of the most important requirements of carriers for potential pharmaceutical applications is high cytocompatibility. To evaluate the cytocompatibility of **CHEMSPOx** and **CHEMSPOx-coumarin** vesicles, their cytotoxicity was evaluated over a broad range of polymer concentrations from 10 to 2500 µg mL^{-1} in PBS. Both polymers revealed a cytocompatibility with a toxic concentration (IC_{50}) of 800 to 1140 µg mL^{-1} for **CHEMSPOx** and **CHEMSPOx-coumarin** (**Figure 3**). This is in line with the results of other structure-related lipopoly(oxazoline)s, e.g., lipopoly(oxazoline)s evaluated on mouse fibroblasts (NIH 3T3) revealed a IC_{50} value of 450 µg mL^{-1} with linear saturated POx (C_{16}POx) and 20.24 mg mL^{-1} with linear unsaturated ($C_{18:2}$POx).[40] Below a polymer concentration of 100 µg mL^{-1} **CHEMSPOx** and **CHEMSPOx-coumarin** show similar high cytocompatibility. Above this concentration, however, a significant difference was found between the two polymers ($p < 0.05$) (Figure S20, Supporting Information). This led to the assumption that the significant difference in cytotoxicity is related to the additional coumarin functionalization that altered the physiochemical properties (e.g., hydrophobicity) or due to the anticancer properties of coumarin.[41]

2.3.2. Cellular Internalization of CHEMSPOx Vesicles

To assess the cellular internalization of the **CHEMSPOx** and **CHEMSPOx-coumarin** vesicles, the hydrophobic neutral lipid orange (NLO) was used as a model for hydrophobic drugs. NLO is a solvatochromic dye, which increases its fluorescence signal in a hydrophobic environment. Both polymers revealed efficient and comparable encapsulation efficiencies for NLO, reaching nearly 100 % (Table S4, Supporting Information). Both formulations revealed non-significant changes in size after NLO loading (Z-average of 106 ± 3.4 nm without to 104 ± 0.2 nm with NLO for **CHEMSPOx** and of 96 ± 1.2 nm without to 124 ± 2.2 nm with NLO **CHEMSPOx-coumarin**) (Figure S21, Supporting Information).

For the internalization study, cells were co-incubated with 500 µg mL^{-1} of NLO-loaded vesicles. Since 500 µg mL^{-1} of NLO-loaded vesicles could have an impact on cell viability, an additional PrestoBlue experiment was conducted with different polymer concentrations. The result reveals no impact on cell viability after 1 h incubation (Figure S22, Supporting Information) and underlines the time-dependency of cytotoxicity. The kinetics of the cellular internalization was observed under confocal laser scanning microscopy over 60 min at 37 °C (**Figure 4A**). The staining with Hoechst (in blue) allowed cell localization as well as assessment of cell viability during the experiment. The cellular internalization of NLO-loaded vesicles results in an increase in NLO-fluorescence signal (red) over time. Interestingly, the uptake started within the first 5 min, as illustrated by the videos of the kinetics study (Videos S1 and S2, Supporting Information), where cells were imaged every 5 min. After 5 min, the NLO signal was observed in the cytoplasm for both materials **CHEMSPOx** and **CHEMSPOx-coumarin** and gradually increased over 1 h as reflected by the relative MFI (rMFI) to the maximum detected MFI (Figure 4B). The rMFI over time revealed a fast-exponential internalization kinetic from 15 to 45 min then reached a plateau with the saturation of the fluorescent probes. Both NLO-loaded formulations revealed a similar kinetic despite the additional coumarin group in **CHEMSPOx-coumarin**.

To gain a deeper insight into the internalization mechanism, NLO-loaded vesicles of both polymers were applied to cells at 500 µg mL^{-1} for 1 h, followed by quantification via flow cytometry. Cells were incubated at 4 and 37 °C to discriminate between energy-independent and energy-dependent uptake mechanisms respectively.

After 1 h of incubation, both CHEMSPOx(NLO) and CHEMSPOx-coumarin(NLO) showed a fast uptake with 100% NLO-positive cells (Figure S23, Supporting Information)

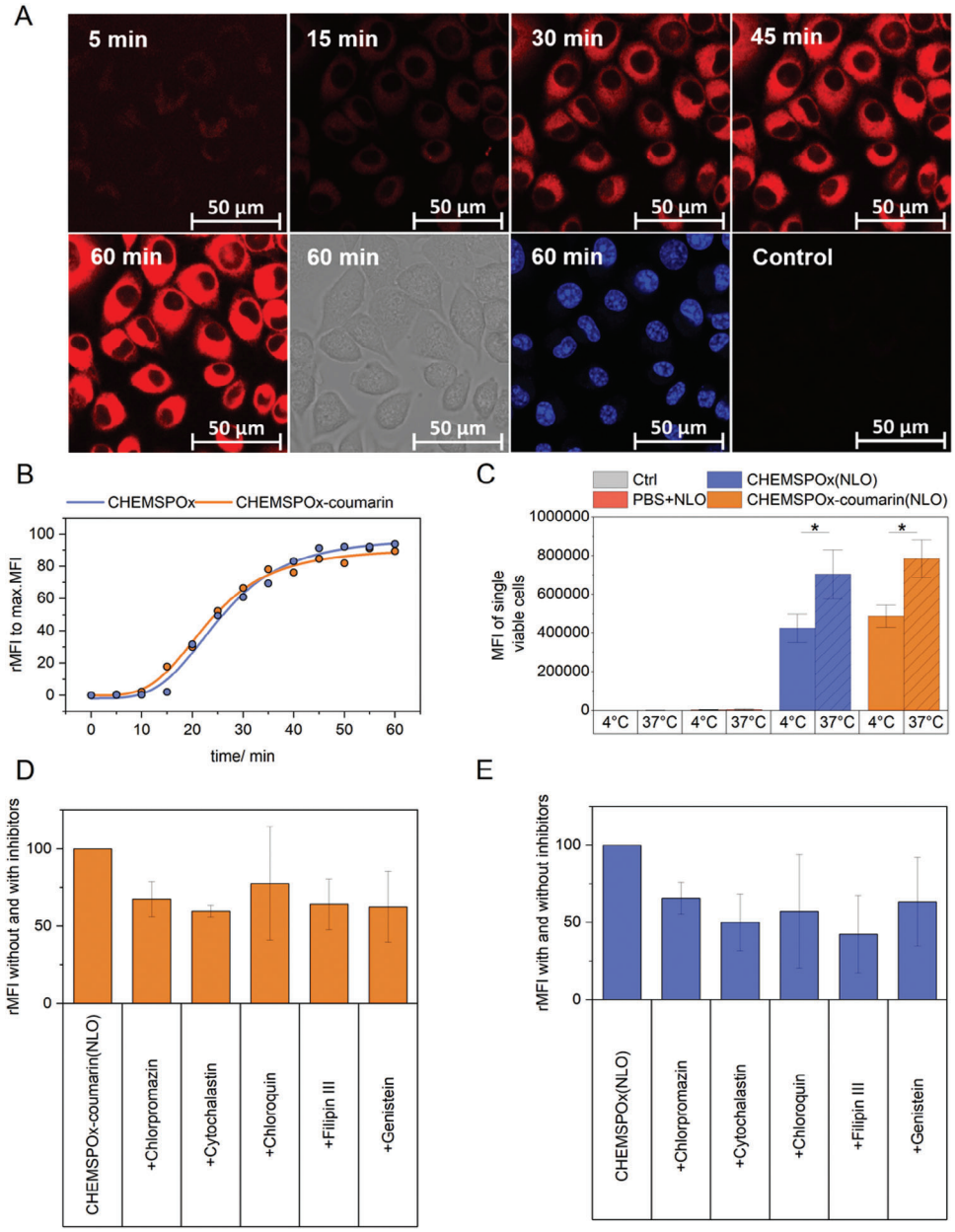

Figure 4. A) Cell internalization kinetics study of **CHEMSPOx** with laser scanning microscopy (LSM) using 40x magnification over 1 h. NLO-loaded vesicles are illustrated in red and the nucleus, stained with Hoechst is illustrated in blue. B) The kinetics of the uptake study conducted with LSM over 1 h is illustrated by the relative mean fluorescence intensity of NLO (rMFI) over 1 h (Equation 4). C) Mean fluorescence intensity (MFI) of viable single cells of CHEMSPOx(NLO) and CHEMSPOx-coumarin(NLO) internalization assay in L929 cells over 1 h at 37 °C vs 4 °C. Statistical analysis was performed using a two-sample *t*-test with equal variance between the 37 °C and 4 °C ($n = 3$). Statistical significance was notated as $^{*}p \leq 0.05$. Video of the kinetic study can be found in Video S1 (Supporting Information). D) Cell internalization on L929 with and without inhibitors reflected by the relative mean fluorescence intensity (rMFI) of CHEMSPOx(NLO) and E) CHEMSPOx-coumarin (NLO).

independent of the incubation temperature. The high percentage of NLO-positive cells at 4 °C suggested, that the uptake of NLO-loaded vesicles is not only based on an active uptake mechanism but also on an energy-independent uptake mechanism, e.g., direct membrane fusion.[42] The direct membrane fusion could be triggered by the interaction of the cholesterol in the polymer structure with the cholesterol on the cell membrane.[43]

Nevertheless, looking at the MFI value, a significantly lower uptake was observed when cell metabolism was slowed down at 4 °C in comparison to the incubation at 37 °C (Figure 4C). Interestingly, similar uptake results were observed on the human embryonic kidney cell line (HEK293T) (Figure S24, Supporting Information) evidencing a cell type-independent fast uptake or membrane fusion.

To identify the internalization pathway of **CHEMSPOx** and **CHEMSPOx-coumarin** vesicles an endocytosis inhibition study was performed. L929 cells were pre-incubated with chemical inhibitors of the endocytic route, such as chlorpromazine (inhibitors for clathrin), Filipin III (inhibiting the lipid raft and caveolae pathway), Genistein (tyrosine kinase inhibitor), cytochalasin D (actin inhibitor) and chloroquine (affecting the function of clathrin and inhibiting endosomal acidification) (Figure S25, Supporting Information).[44,45] The results illustrated in Figure 4D for CHEMSPOx(NLO) and Figure 4E for CHEMSPOx-coumarin(NLO) showed a global but not significant decrease in cell internalization compared to the control for all inhibitors. These results suggest multiple endocytosis pathways for CHEMSPOx(NLO) and CHEMSPOx-coumarin(NLO). Moreover, it is now well established that deciphering the endocytosis phenomenon is particularly challenging, especially regarding recent advances in the understanding of endocytosis mechanisms in eucaryotic cells.[44,46]

Although no clear endocytosis mechanism was identified, it is evident that **CHEMSPOx** and **CHEMSPOx-coumarin** vesicles enable fast internalization in comparison to studied PEGylated nanoparticles[47,48] and revealed a high cytocompatibility due to active multiple endocytosis pathways at 37 °C and via membrane fusion at 4 °C. Interestingly, the fast (within 5 min), energy-dependent cellular uptake was also observed with a set of POx amphiphiles composed of 2-butyl-2-oxazoline, 2-nonyl-2-oxazoline, 2-n-propyl-2-oxazoline, 2-isopropyl-2-oxazoline (iPrOx) as the hydrophobic blocks.[49]

The results led to the assumption that the observed fast internalization is attributable to the cholesterol part of the polymer structure. It is known that hydrophobicity in the carrier structure enhances cellular internalization and can be used as penetrating ligands.[50] Its integration into the polymer structure leads to improved hydrophobicity and, consequently, improved internalization due to its possible interaction with the cell membrane, without destroying the membrane. The cholesterol anchor may trigger the uptake via lipid raft-dependent endocytosis, as well as it could interact with steroid receptors or cholesterol on the cell membrane surface.[38,51,52] This inherent feature of the cholesteryl anchor could be responsible for the high cytocompatibility and the fast internalization of **CHEMSPOx** and **CHEMSPOx-coumarin** vesicles and their cargo.

Overall, the **CHEMSPOx** and **CHEMSPOx-coumarin** vesicles enable fast internalization in comparison to studied PEGylated nanoparticles.[47,48] To further investigate the membrane interaction, hemolysis and aggregation assay were conducted on human erythrocytes.

2.3.3. Hemolysis and Aggregation Assay

An effective uptake often correlates with intense interaction with the cell membrane. To evaluate the polymer-cell membrane interaction in more detail, a hemolysis assay was performed with the polymer at concentrations ranging from 100 to 2350 µg mL^{-1}. **Figure 5A** demonstrated high membrane compatibility for **CHEMSPOx** and **CHEMSPOx-coumarin** up to the highest, tested polymer concentration, albeit **CHEMSPOx** was getting slightly hemolytic at concentration >1000 µg mL^{-1} (hemolysis relative to Triton < 5 %). Moreover, both polymer candidates showed low aggregation rates (Figure 5C). The results emphasized the safety profile of **CHEMSPOx** and **CHEMSPOx-coumarin** for biological applications.

In addition, further characterization of membrane-polymer interaction was conducted. The ability of the polymer to protect the cellular membrane was investigated by the addition of the cationic hemolytic agent hexadecyltrimethylammonium bromide (CTAB).[53] Figure 5B demonstrated a significant membrane protection property of the polymers at a concentration of 500 µg mL^{-1} for **CHEMSPOx** and 100 µg mL^{-1} for **CHEMSPOx-coumarin**. Additionally, the membrane-protecting property was investigated in biological duplicate with the membrane-active material Eudragit EPO (Figure S26, Supporting Information) and demonstrated a similar effect. The outcome is considered to be a result of a synergistic effect of poly(2-methyl-2-oxazoline) and cholesterol. As cholesterol is crucial for the cellular membrane structure and function, the cholesterol anchor in **CHEMSPOx** and **CHEMSPOx-coumarin** might be incorporated and prevent membrane disruption leading to protection against full membrane destruction. This feature of **CHEMSPOx** and **CHEMSPOx-coumarin** can be used for applications where biological membranes should be protected or preserved. Moreover, the outcome emphasized the ability of **CHEMSPOx** and **CHEMSPOx-coumarin** to enable and trigger membrane fusion due to the integration in the cell membrane. This leads to accelerated particle transport through the cell membrane, which happened also at low cultivation temperatures (4 °C).

3. Conclusion

This work aimed at evaluating the potential of a lipopoly(oxazoline) for efficient intracellular delivery. A cholesteryl hemisuccinate group (CHEMS) as lipid anchor was grafted on poly(2-methyl-2-oxazoline) by ω-functionalization (**CHEMSPOx**). For further investigation of the functionalization potential of the polymer, a coumarin group was also added successfully to the structure using a coumarin-functionalized initiator (**CHEMSPOx-coumarin**) for the first time. Due to the amphiphilic character of the polymers, they self-assembled into multilamellar and unilamellar vesicles with a size of ≈100 nm when simply dissolved in water. For biological investigation, the high cytocompatibility of the assemblies was ensured via PrestoBlue assay. A detailed characterization of the intracellular delivery potential of the vesicles was performed using NLO as a hydrophobic dye that accumulated in the hydrophobic core of the vesicles. The NLO-loaded vesicles revealed fast intracellular delivery independent from used cell lines (L929 and HEK293T). Within 5 min after addition at 37 °C, NLO enrichment in the cell could be detected via LSM and started to saturate after 40 min and this efficient intracellular delivery was also demonstrated at 4 °C for both formulations. Thus, a complex mixture of different internalization pathways was involved in active uptake such as endocytosis but also probably non-energy dependent mechanisms such as membrane fusion (possible mechanism illustrated in **Figure 6**). To elucidate the mechanism of the fast and efficient internalization, an endocytosis inhibition assay was conducted with chemical inhibitors. The outcome led to the conclusion that multiple internalization pathways are

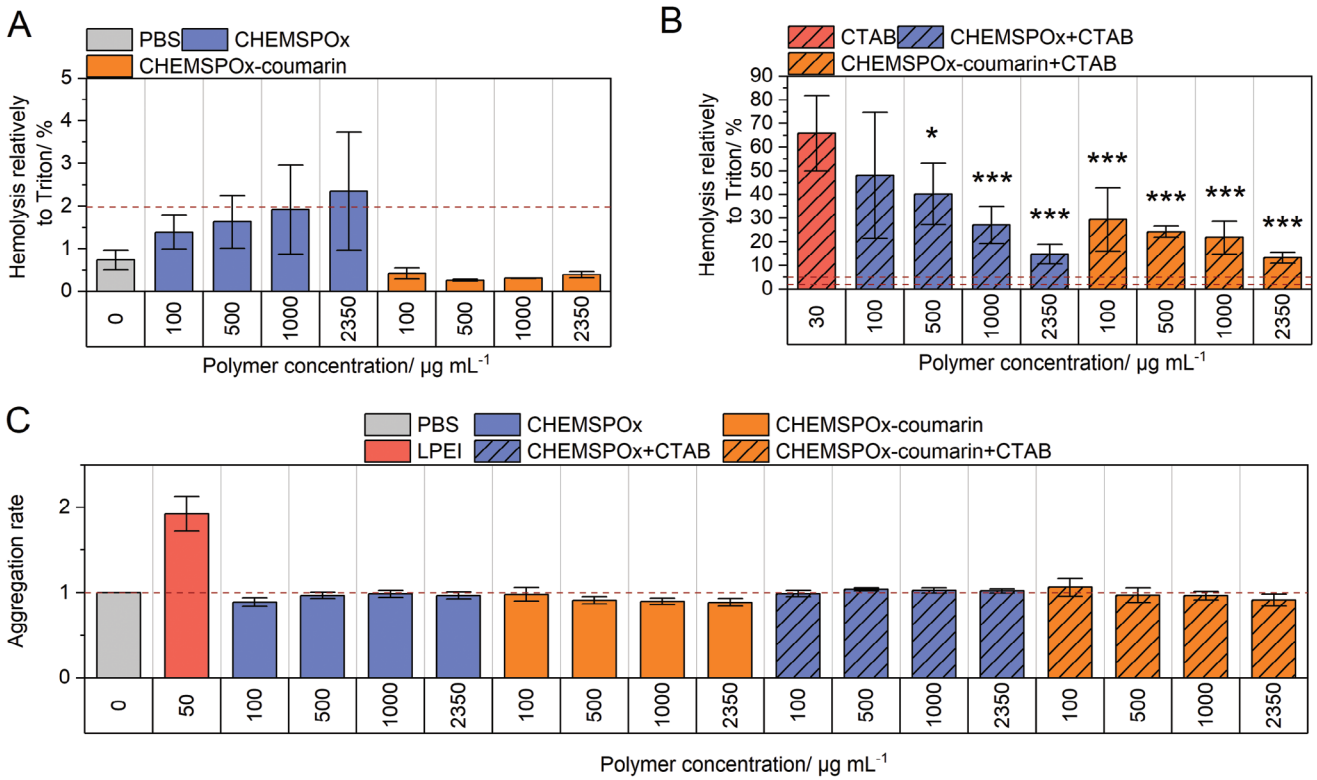

Figure 5. A) A hemolysis assay was performed at pH 7.4 to investigate the polymer-cell membrane interaction. Hemolysis between 2% and 5% is considered non-hemolytic and slightly hemolytic, respectively. B) Hemolyis-protection property of tested polymers with the addition of 30 µg mL^{-1} CTAB. The stronger the interaction, the higher the amount of released hemoglobin calculated relative to the positive control Triton X-100. Statistical analysis was performed using a two-sample *t*-test with equal variance between the CTAB-treated samples and CHEMSPOx+CTAB and CHEMSPOx-coumarin+CTAB treated. Statistical significance was notated as $^{*}p \leq 0.05$, $^{**}p \leq 0.01$, and $^{***}p \leq 0.001$. C) Aggregation assay. All values of hemolysis and aggregation assays represent the mean ± SD ($n \leq 3$) of different donors.

involved in the uptake process. Finally, the membrane interaction and hemocompatibility were studied in detail. The high membrane compatibility was underpinned by the results of the hemolysis and aggregation assays. Moreover, **CHEMSPOx** and **CHEMSPOx-coumarin** evidenced their membrane protective effect in the presence of the membrane-disrupting agent CTAB. These results, open further interesting application fields of lipopoly(oxazoline), where biological membranes should be protected or preserved, and an intravenous administration could be considered. This initial study has highlighted the substantial potential of **CHEMSPOx** such as enabling fast intracellular drug delivery or exhibiting protective effects on membranes. With the capability for functionalization without compromising the polymer's biological properties, exemplified by the integration of biologically active drugs like coumarin, **CHEMSPOx** provides an ideal basis for such applications and beyond.

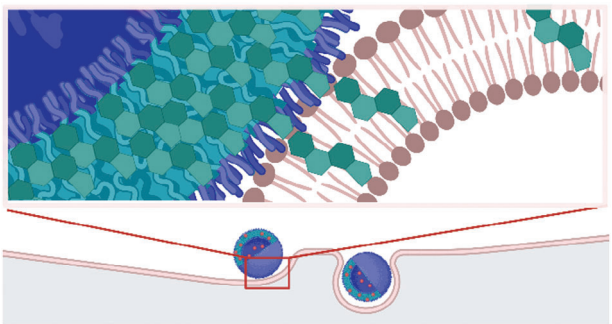

Figure 6. Proposed mechanism of membrane interactions based on a cholesterol anchor supporting the uptake. Interaction with cholesterol on the cell membrane surface leads to fast internalization.

4. Experimental Section

Material: The following materials were received from Sigma Aldrich (Germany) for synthesis purposes: Methyl *p*-toluenesulfonate (MeOTs), 2-methyl-2-oxazoline, cholesteryl hemisuccinate, *N,N′*-dicyclohexylcarbodiimide (DCC), 4-(dimethylamino)pyridine (DMAP), 4-methylumbelliferone, potassium carbonate (K2CO3), 2-bromo-ethanol, *p*-toluenesulfonyl chloride (TsCl), triethylamine, anhydrous magnesium sulfate, methanolic potassium hydroxide solution (KOH/MeOH), dry acetonitrile, diethyl ether, anhydrous dichloromethane, *N,N*-dimethylformamide, ethanol, chloroform. Spectra/Por 6 dialysis membranes pre-wetted RC tubing with 500 Da MWCO were brought from Spectrum Labs (USA).

For biological investigations all the following materials were ordered from the suppliers stated in brackets: TC-treated cell culture flasks and 96-U-bottom well plate (Greiner Bio-One International GmbH and Labsolute, Th. Geyer GmbH & Co. KG), TC-treated multi-well cell culture plates (VWR International GmbH), µ-Plate 24-well Black (ibidi GmbH, Germany)

or µ-Slide 8-well high glass bottom (ibidi GmbH, Germany), L929 cells (CLS Cell Lines Service GmbH, Eppelheim, Germany) HEK293T (DSMZ, Braunschweig, Germany), Dulbecco's modified eagle medium (DMEM), phosphate-buffered saline pH 7.4 (PBS), fetal bovine serum (FBS), Trypsin-EDTA and Penicillin-Streptomycin were purchased from Capricorn Scientific GmbH, Germany. Opti-MEM™ reduced serum medium and PrestoBlue cell viability reagent, Hoechst, Transferrin from Human Serum, Alexa Fluor 633 Conjugate and BODIPY FL C5-Lactosylceramid (Thermo Fisher Scientific), linear poly(ethylene imine) (LPEI, 25 kDa, Polysciences), brached poly(ethylene imine) (BPEI, Mw = 10 kg mol-1, Polysciences, Germany). Human blood was obtained from the Department of Transfusion Medicine of the University Hospital, Jena. Hanks' Balanced Salt Solution without calcium and magnesium (HBSS), dimethylsulfoxid (DMSO), Triton X-100, hexadecyltrimethylammonium bromide (CTAB), chloroquine diphosphate, Filipin III, cytochalasin D, genistein and chlorpromazine-hydrochloride (Sigma–Aldrich, USA), neutral lipid orange (NLO) (Dyomics GmbH, Jena, Germany), inhibitors, sodium acetate, sodium chloride (Grüssing GmbH, Germany), Immersol V 2010 (Immersion Oil) (Carl Zeiss GmbH, Germany), Rotilabo-syringe filters, cellulose mixed esters filters sterile (Carl Roth GmbH).

Synthesis of POx-OH by Cationic Ring-Opening Polymerization: Cationic ring-opening polymerization was carried out under a dry nitrogen atmosphere. Methyl p-toluene sulfonate (0.186 g, 1 mmol) and 2-methyl-2-oxazoline (MOx) (4.25 g, 50 mmol) were dissolved in dry acetonitrile (30 mL). The solution was vigorously stirred at 80 °C for 24 h. Then, the polymerization was quenched at 40 °C by the addition of an adequate amount of methanolic potassium hydroxide solution (15 mL at 2 mol L^{-1}). The flask was maintained at 40 °C overnight. After cooling, the reaction mixture was concentrated and then the poly(2-methyl-2-oxazoline) (POx-OH) was obtained after two successive precipitations in cold diethyl ether. Finally, the polymer was dissolved in water (10 mL) and freeze-drying led to the obtaining of the POx-OH as a fully dry white powder (yield: 84%). The NMR spectrum in D_2O of this molecule was added in Figure S1 (Supporting Information): ^{1}H NMR (400 MHz, D_2O, δ): 3.44–3.62 (4H, H_b), 3.10 (3H, H_a), 2.18–2.09 (3H, H_c). The $DP_{n,\,exp}$ value was also calculated from the terminal CH_3 (H_a on Figure S1, Supporting Information) at 3 ppm versus the CH_2 of POx repetitive unit at 3.5 ppm.

Esterification with Cholesteryl Hemisuccinate (CHEMS): An anhydrous dicloromethane solution (35 mL) of cholesteryl hemisuccinate (CHEMS) (1.2 eq, 2.3 mmol) was added to another anhydrous dichloromethane solution (50 mL) containing POx-OH (1 eq, 1.92 mmol), DCC (1 eq, 1.92 mmol) and DMAP (0.25 eq, 0.48 mmol) under ice bath. The mixture was stirred for 24 h at room temperature. Then the solvent was removed by vacuum and the crude product was dialyzed for three days through a 500 Da take-off membrane. Finally, the polymer dissolved in water was freeze-dryed and led to the final CHEMSPOx as a fully dry white powder (yield: 65%). The NMR spectrum in $CDCl_3$ of this molecule was added in Figure S2 (Supporting Information): ^{1}H NMR (400 MHz, $CDCl_3$, δ): 5.35 (1H, H_5), 4.51 (1H, H_3), 3.44–3.62 (4H, H_b), 3.10 (3H, H_a), 2.61-2.55 (4H, H_1 and H_2), 2.33 (2H, H_4), 2.18–2.09 (3H, H_c), 1.96-1.01 (18H, H_{CHEMS}), 0.95 (3H, H_{10}), 0.89 (3H, H_8), 0.82 (6H, H_6 and H_7), 0.66 (3H, H_9). The efficiency of functionalization F% was calculated based on Figure S2 (Supporting Information) by comparing the pic (a) related to -CH_3 of the initiator that integrates for $\int_{int}$ a = 1, and the pic 9 of a -CH_3 of the cholesterol that integrates for $\int_{int}$ 9 = 0.85, given a functionalization efficiency of F% = 87%.

Synthesis of Poly(Oxazoline)s with Coumarin Grafting CHEMSPOx-Coumarin—Synthesis of Coum-Ethyl-OH: 4-Methylumbelliferone (1 eq, 34 mmol), K_2CO_3 (0.7 eq, 23.8 mmol), and 2-bromo-ethanol (1.5 eq, 51.1 mmol) were dissolved in DMF (0.25 M). The mixture was heated at 85 °C for 20 h before being cooled and precipitated in diethyl ether. The crude product was filtered, dried under a vacuum, and recrystallized from ethanol. After filtration and drying under vacuum, a white powder was obtained in a 75% yield. The NMR spectrum in $CDCl_3$ of this molecule was added in Figure S3 (, Supporting Information): ^{1}H NMR (400 MHz, $CDCl_3$, δ): 7.54 (d, 1H, H_3), 6.88 (d, 1H, H_4), 6.85 (s, 1H, H_7), 6.17 (s, 1H, H_6), 4.15 (d, 2H, H_1),4.02 (d, 2H, H_2), 2.41 (s, 3H, H_5).

Synthesis of Poly(Oxazoline)s with Coumarin Grafting CHEMSPOx-Coumarin—Tosylation of Coum-Ethyl-OH to Obtain the Initiator Coum-Ethyl-OTs: An anhydrous dichloromethane solution (1 M) of TsCl (1.1 eq, 12.4 mmol) was added dropwise at 0 °C to a chloroform solution (1 M) of Coum-ethyl-OH (1 eq, 11.35 mmol) and triethylamine (2.2 eq, 24.9 mmol). The resulting solution was stirred at room temperature for 24 h, filtered, and washed with brine (3×). The organic phase was dried over anhydrous MgSO4 and concentrated under reduced pressure. Recrystallization from diethyl ether gave a white powder with a 60% yield. The NMR spectrum in $CDCl_3$ of this molecule was added in Figure S4 (Supporting Information): ^{1}H NMR (400 MHz, $CDCl_3$, δ): 7.82 (d, 2H, H_3 and H_5), 7.46 (d, 1H, H_9), 7.36 (d, 2H, H_2 and H_4), 6.89 (d, 1H, H_8), 6.63 (s, 1H, H_{12}), 6.12 (s, 1H, H_{11}), 4.40 (t, 2H, H_6), 4.15 (d, 2H, H_7), 2.47 (s, 3H, H_{10}), 2.39 (s, 3H, H_1).

Synthesis of Poly(Oxazoline)s with Coumarin Grafting CHEMSPOx-Coumarin—Synthesis of Coum-POx-OH: Polymerizations were carried out under a dry nitrogen atmosphere. The initiator Coum-ethyl-OTs (1 eq, 3.2 mmol) and MOx (50 eq, 80.2 mmol), were dissolved in dry acetonitrile (4 M). The solution was vigorously stirred at 80 °C for 24 h. The product was quenched by the addition of an adequate amount of methanolic potassium hydroxide (5 eq, 5 M). The flask was maintained at 40 °C for 12 h. After cooling, the polymer was isolated by slow precipitation from cold diethyl ether (with a yield of 82%). The NMR spectrum in $CDCl_3$ of this molecule was added in Figure S5 (Supporting Information): ^{1}H NMR (400 MHz, $CDCl_3$), δ): 7.41 (1H, H_4), 6.81 (1H, H_3), 6.75 (1H, H_7), 6.24 (1H, H_6), 4.15 (2H, H_1), 3.70 (2H, H_2), 3.20–3.70 (4H, H_a), 2.33 (3H, H_5), 2.12–1.85 (3H, H_b). The experimental degree of polymerization ($DP_{n,\,exp}$) was calculated by ^{1}H NMR spectroscopy using the integration of H_6 (assignment on Figure S5, Supporting Information) of the terminal coumarin unit related to the CH_2 of POx repetitive unit at 3.5 ppm.

Synthesis of Poly(Oxazoline)s with Coumarin Grafting CHEMSPOx-Coumarin—Esterification with cholesteryl hemisuccinate (CHEMS): An anhydrous dichloromethane solution (20 mL) of cholesteryl hemisuccinate (CHEMS) (1.2 eq, 1.67 mmol) was added to another anhydrous dichloromethane solution (35 mL) containing Coum-POx-OH (1 eq, 1.3 mmol), DCC (1 eq, 1.3 mmol) and DMAP (0.25 eq, 0.34 mmol) under ice bath. The mixture was stirred for 24 h at room temperature. Then the solvent was removed by vacuum and the crude product was dialyzed for three days through a 500 Da take-off membrane. Finally, the polymer was freeze-drying leading to the obtaining of the Coum-POx-CHEMS as a fully dry white powder (yield: 56 %). The NMR spectrum in $CDCl_3$ of this molecule was added in Figure S6 (Supporting Information): ^{1}H NMR (400 MHz, $CDCl_3$), δ): 7.51 (1H, H_3), 6.81 (2H, H_4 and H_5), 6.14 (1H, H_1), 5.35 (1H, H_{12}), 4.50 (1H, H_{10}), 4.16 (2H, H_7), 3.75 (2H, H_6), 3.62-3.33 (4H, H_a), 3.10-2.20 (6H, H_8, H_9 and H_{11}), 2.35 (3H, H_2), 2.22-1.95 (3H, H_b), 1.90-0.90 (24H, H_{15}, H_{17} and d rest of H_{CHEMS}), 0.81 (6H, H_{13} and H_{14}), 0.64 (3H, H_{16}).

The efficiency of functionalization F% was calculated based on Figure S6 (Supporting Information) by comparing the pic (3) or (1) related to -CH_3 of the Coumarin that integrates for $\int_{int}$ a = 1, and the pic 12 of a -CH_3 of the cholesterol that integrates for $\int_{int}$ 9 = 0.9, given a functionalization efficiency of F% = 90%.

^{1}H NMR Spectroscopy: ^{1}H NMR was recorded using a Bruker Advance DRX 400 (400 MHz) using $CDCl_3$ as a deuterated solvent. Chemical shifts were given in parts per million (ppm) for ^{1} H NMR the reference peak relative to the residual proton signal of the nondeuterated solvent $CHCl_3$ and D_20 was at 7.26 and 4.79 ppm respectively.

Size Exclusion Chromatography (SEC): Molar masses and dispersity of polymers were determined by size exclusion chromatography (SEC) using a PL-GPC50 Plus equipped with an RI refractive index detector. Polar Gel M column was used at 50 °C with a dimethylacetamide (DMAc) (+ 0.1 % LiCl weight) flow rate of 0.8 mL min^{-1}, calibrated with PMMA standards.

Determination of Critical Aggregation Concentration: Critical aggregation concentrations (CAC) were determined by fluorescence measurements at 25 °C with a Tecan Infinite M200 PRO microplate reader, using Nile Red. The polymers were dissolved in PBS at a concentration ranging from 0.004 to 1 mg mL^{-1}. Six microliters Nile Red (0.1 mg mL^{-1} in THF) was added to 0.5 mL of each formulation and incubated for 6 h at room

temperature to evaporate residual THF. For the measurement, 200 µL of each sample was transferred to a 96 well-plate. The fluorescence was measured from 550 to 724 nm in 2 nm steps (λ_{Ex} = 535 nm). For CAC determination, the intensity at 640 nm of each fluorescence emission spectra was plotted versus the micelle concentration for each sample. The experiment was performed in technical triplicates. The CAC was determined as the intersection point in the plot of the maximum fluorescence emission versus the polymer concentration. The plotting and calculation were performed with OriginPro2022b.

Polymer Vesicles Preparation: After investigation of different formulation methods, the direct dissolution in water was selected as the most suitable process without the organic solvent requirement (Figure S7, Supporting Information). The solution of CHEMSPOx and CHEMSPOx-coumarin were prepared at 2.5 g L^{-1} by direct solubilization in water. After 24 h of magnetic stirring the solution was filtered through 0.22 µm (cellulose mixed esters filter). The scattered intensity of the polymer solution before and after filtration was checked to ensure that most of the original solution remained.

Dynamic Light Scattering, Static Light Scattering, and Nanoparticle Tracking Analysis: Z-average and polydispersity index (PDI) were measured using a Zetasizer NanoZS apparatus (Malvern Instruments, UK) equipped with a He-Ne laser (wavelength: 632.8 nm) at a temperature of 25 °C and a scattering angle of 173° for detection. Size measurements were performed in water. All the results are the average of three independent measurements (with three different stock solutions prepared).

Static Light Scattering (SLS) analyses were performed using a compact ALV-CGS3 goniometer with an ALV/LSE-5004 light scattering electronics and an ALV-7004 multi-tau digital correlator with pseudo-cross correlation detection (ALV-Laser Vertriebsgesellschaft mbH, Langen, Germany). The light source was a 22 mW He-Ne laser operating at λ = 632.8 nm. The analysis was carried out at 25 °C with angles ranging from 25° to 150° by step of 5°. SLS data were treated using the open-access software SASfit. They were analyzed using the form factor of bilayered vesicles. The bilayer thickness was measured on the CryoTEM images (n = 10) and used as a constant. The internal radius and a multiplicative correction factor were used as fitting parameters.

The stability upon dilution of the **CHEMSPOx** and **CHEMSPOx-coumarin** vesicles was analyzed using a NanoSight NS300 (Malvern Instruments, UK) as a complementary method to dynamic light scattering. The solutions were diluted by 1000 with water to obtain a particle concentration in the 1 × 10^8 particles mL^{-1}. Measurements were performed with a 405 nm laser. Samples were analyzed using the NanoSight NTA 3.2 software following a tailored script: the temperature was set at 25 °C, the syringe pump at 40 AU, and three videos of 60 s were recorded. Videos were recorded with a camera level set to 14 and analyzed with a detection threshold set to 5. In order to ease comparison with DLS results, the dispersity of the samples was expressed using the polydispersity index (PDI) calculated with the following Equation (1):

$$\mathrm{PDI} = \left(\frac{\text{Std Dev}}{\text{Mean Size}}\right)^2 \quad (1)$$

Characterization of Coumarin Group Properties: Fluorescence Signal and UV Dimerization: The fluorescence signal of the coumarin grafted onto the **CHEMSPOx** was quantified with a Spectro fluorophotometer (Shimadzu, RF-6000) and a high-precision cell (light path 3 × 3 cm, center 15). The parameters were set up as Bandwidth EX 5 nm and EM 10 nm, scan speed 600 nm min^{-1} and $\lambda_{Ex}/\lambda_{Em}$ on 315/380 nm). To compare the fluorescence intensity and polarity reactivity of the solution at 200 mg L^{-1} were prepared in DPBS. The emission spectrum was obtained from 200 to 600 nm. **CHEMSPOx-coumarin** solution at 2.5 g L^{-1} was irradiated under UV light with a cylindrical photochemical reactor "Rayonnet" composed of 16 symmetrically placed lamps with emission maxima set at 300 nm (UV-B). The samples were irradiated in quartz cuvettes (1 cm × 1 cm × 4.5 cm) placed on a circular rotating holder. Different irradiation times of the **CHEMSPOx-coumarin** solution were tested: 30, 60, and 100 min. To follow the dimerization of the coumarin the absorbance signal was followed with a Perkin Elmer-lambda 35 UV/Vis spectrometer equipped with PTP-1+1 Peltier System.

CryoTEM Observations: CryoTEM measurements were performed on an FEI Tecnai G^2 20 equipped with a LaB6 filament with an acceleration voltage of 200 kV. Samples were prepared on Quantifoil grids (R2/2) which were treated with N2 plasma prior to use for hydrophilization and cleaning. The solution (8.5 µL) was vitrified on Quantifoil grids using a Vitrobot Mark IV system. Liquid ethane was used as a cryogen. Samples were transferred to a Gatan 626 cryo holder and were maintained at a temperature of < 175 °C during the entire process. All images were acquired with a Mega View (OSIS, Olympus Soft Imaging Systems) or an Eagle 4k CCD camera, respectively.

Vesicles Formulation with NLO Loading and Quantification: The solution of **CHEMSPOx** and **CHEMSPOx-coumarin** were prepared at 5 mg mL^{-1} in PBS (pH 7.4). The solution was maintained under agitation overnight using the multi-rotator (Multi-Rotator PTR-35 Grant-bio Fluidlab R-300, Anvajo) to obtain polymer self-assembly. The obtained suspension was then filtered through 0.22 µm (cellulose mixed esters filter). To allow NLO loading, 2 µL NLO solution (1 mg mL^{-1} in DMSO) was added to 1 mL formulation and incubated another 24 h before centrifugation at 10,000 rpm for 10 min (Eppendorf Centrifuge 5804R) to induce sedimentation of non-associated NLO aggregates. The supernatant, containing NLO-loaded particles was used for further experiments. To determine the encapsulation efficiency of NLO, 1 mL of the formulation was frozen at −80 °C and freeze-dried (Alpha 2–4 LD plus) at -75 °C and 0.08 mbar for 24 h. The freeze-dried samples were redissolved in 100 µL milli-Q water, followed by 300 µL DMSO. Since NLO is a solvatochromic dye, which increases its fluorescence signal in a hydrophobic environment, the solution was further diluted 1:4 (v/v) with DMSO. Afterward, the dilutions were transferred in triplicate into a 96-well plate to measure the fluorescence intensity with the multi-plate reader (Tecan infinite M200Pro) at λ_{Ex} = 488/ λ_{Em} = 590 nm. NLO in PBS was used as 100 % control.

The encapsulation efficiency was calculated as in Equation (2):

$$\text{Encapsulation efficiency}/\% = \frac{\mathrm{FI}_{\mathrm{Sample}}}{\mathrm{FI}_{\mathit{free\ NLO}}} \cdot 100 \quad (2)$$

where FI_{Sample}, $FI_{free\ NLO}$ represent the fluorescence intensity of a given sample and the NLO in PBS control (100%), respectively.

Cell Culture: For cultivation of the mouse fibroblast cell line L929 and human embryonic kidney cell line HEK293T cell line Dulbecco's modified Eagle's medium (DMEM, 1 g L^{-1} glucose) supplemented with 10% (v/v) fetal bovine serum (FBS), 100 U mL^{-1} penicillin, and 100 µg mL^{-1} streptomycin (D10) was used. Cells were cultivated at 37 °C in a humidified 5% (v/v) CO_2 atmosphere. One day before the PrestoBlue assay, the L929 cell line was seeded in a 96-well plate at a cell concentration of 0.1 × 10^6 cells mL^{-1} in a total volume of 100 µL per well. For particle uptake studies, 24 h before the experiment L929 was seeded in a 24-well plate at a cell concentration of 0.2 × 10^6 cells mL^{-1} in 500 µL D10. Before cells were treated, a visual cell density of ≈70% was necessary. To study the uptake kinetic with laser scanning microscopy (LSM), L929 cells were seeded in a µ-slide 8-well high glass bottom (ibidi GmbH, Germany) at a cell concentration of 0.2 × 10^6 cells mL^{-1} in 250 µL D10. On the glass bottom and for microscopic investigation, a cell density of ≈50% was aimed. For cell counting Fluidlab R-300 anvajo was used.

Determination of Metabolic Activity in L929 Cells (PrestoBlue Assay): For the determination of cytotoxicity of the **CHEMSPOx** and **CHEMSPOx-coumarin** PrestoBlue assay was applied. Therefore, the unloaded polymer vesicles were used. The assay is a calorimetric-based method, which assesses the metabolic activity of viable mouse fibroblast cell line L929 and was performed following ISO10993-5. One hour before treatment the medium was changed to 50 µL fresh Dulbecco's modified Eagle's medium (DMEM, 1 g L^{-1} glucose) supplemented with 20% (v/v) fetal bovine serum (FBS), 100 U mL^{-1} penicillin, and 100 µg mL^{-1} streptomycin (D20). Cells were treated with 50 µL **CHEMSPOx** and **CHEMSPOx-coumarin** diluted in PBS buffer. The tested concentration ranges from 10 to 2500 µg mL^{-1}. LPEI was used as a positive control at a concentration

of 10 to 100 µg mL^{-1}. After 24 h of incubation, the medium was replaced by a 10% (v/v) PrestoBlue solution in a fresh D10, prepared according to the manufacturer's instructions. Furthermore, 1 h incubation was investigated to assess the time-dependent cellular viability. Cells were further incubated at 37 °C for 45 min and the fluorescence was measured with the multi-plate reader (Tecan Infinite M200Pro, Germany) at λ_{Ex} = 570 / λ_{Em} = 610 nm. With PBS treated control cells on the same plate were defined to 100% viability. The relative number of viable cells was calculated as in Equation 3:

$$\text{Rel.viability}/\% = \frac{\text{MFI}_{\text{Sample}} - \text{MFI}_0}{\text{MFI}_{\text{Ctl}} - \text{FI}_0} \cdot 100 \quad (3)$$

where $\text{FI}_{\text{Sample}}$, FI_0, and FI_{Ctrl} represent the fluorescence intensity of a given sample, medium without cells (the blank), and PBS buffer-treated control (100% viability), respectively. The toxic concentration (IC_{50}) was calculated with OriginPro 2022b software using a non-linear dose-response function. More details can be found in Equation S1, Figure S8, and Table S1 (Supporting Information). The assay was performed in three biological replicates.

Microscopic Investigation of the Vesicle Uptake Kinetic: To investigate the vesicle uptake kinetic, mouse fibroblast cells L929 were seeded in a µ-slide 8-well high glass bottom (ibidi GmbH, Germany) and preincubated for 24 h for attachment. Before treating, cells were stained with Hoechst (1:1000 (v/v)) for 10 min and washed with 250 µL warm PBS. 225 µL D10 followed by 25 µL of the NLO encapsulated formulation was added to each well. Cells were imaged immediately using LSM 800, Elyra PS.1 system (ZEISS, Germany). NLO was excited at 561 nm using emission filters for 585 to 733 nm. For magnification, C-Apochromat 40×/1.2 W Korr FCS M27 objective was used. Images were acquired using the ZEN software, version 2.3 SP3 (Zeiss, Jena, Germany), and were processed using the ZEN software (Version 3.4) (Equation S2, Supporting Information). The MFI is detected from LSM and is an output parameter calculated from ZEN software, version 2.3 SP3. The relative mean fluorescence intensity (rMFI) is calculated for plotting as follows:

$$\text{rMFI} = \frac{\text{MFI}}{\text{MFI max}} \cdot 100 \quad (4)$$

where MFI and MFI max are the MFI of the sample at a specific time point and the maximum MFI after 1 h of incubation detected, respectively.

Vesicle Uptake Study in L929 Cells: Mouse fibroblast cell line L929 was treated with 500 µg mL^{-1} of the NLO-loaded particles for 1 h at 37 °C. In parallel, cells and nanoparticles are incubated at 4 °C to inhibit endocytosis processes and identify the proportion of cellular internalization attributable to this entry mechanism. The assay was performed in D10. After the incubation, cells were treated with 150 µL Trypsin-EDTA for 5 min before the trypsinization was stopped with 350 µL serum-containing media (D10). The cell suspension was then transferred to a 96 U-bottom well plate and centrifuged for 5 min at 1000 g and 4 °C with Eppendorf Centrifuge 5804R. After this step, all steps were carried out at 4 °C. The plate was gently swiveled upside down to remove the supernatant and cell pellets were washed thrice with 200 µL PBS. For analysis, cell pellets were resuspended in 200 µL PBS w/o calcium and measured via flow cytometry (Beckmann Coulter, Brea, CA, U.S.) at λ_{Ex} = 488 nm combined with a 585/42 nm bandpass filter. Viable single cells were gated according to the FSC/SSC pattern of the control treated with only PBS buffer. NLO-positive cells were gated to the PBS + NLO control to exclude the enrichment of the solvatochromic NLO dye in hydrophobic cell compartments. The gating strategy can be found in Figure S9 (Supporting Information).

Endocytosis Inhibition Assay: Mouse fibroblast cells L929 were incubated with 500 µL inhibition solutions prepared in Opti-MEM reduced serum medium for 2 h at 37 °C and 5% (v/v) CO_2 atmosphere. The composition and concentration of the inhibitor dilutions can be found in Table S2 (Supporting Information). For each inhibitor, the concentration was chosen regarding the cytocompatibility determined via PrestoBlue assay as described in the method section 2.2.13 and the inhibition effect (with Alexa Fluor 633 conjugated transferrin from human serum, and BODIPY™ FL C5-Lactosylceramid as positive controls) as published.[54–56] The results of cytocompatibility are shown in Figure S10 (Supporting Information). Afterward, cells were treated with a fresh media containing inhibitors supplemented with 500 µg mL^{-1} of the NLO-loaded particles and incubated for 30 min at 37 °C and 5% (v/v) CO_2 atmosphere. After incubation, cells were harvested using Trypsin-EDTA and transferred to a 96-well plate. Three washing steps using HBSS and centrifugation at 1000 rpm, 4 °C, for 5 min were performed before flow cytometry analysis (Beckmann Coulter, Brea, CA, U.S.) at λ_{Ex} = 488 nm combined with a 585/42 nm bandpass filter. Viable single cells were gated according to the FSC/SSC pattern of the control treated with only PBS buffer. Values of cell internalization were obtained as follows:

$$rMFI = \frac{\text{MFI}_{\text{Sample+inhibitor}}}{\text{MFI}_{\text{Sample}}} 100 \quad (5)$$

where $\text{MFI}_{\text{Sample+inhibitor}}$ and $\text{MFI}_{\text{Sample}}$ are the cell fluorescence intensity of cells treated with CHEMSPOx(NLO) and CHEMSPOx-coumarin(NLO) with inhibitors addition and without inhibitors, respectively.

Hemolysis and Aggregation Assay: The erythrocyte aggregation and hemolysis were performed according to a previously published protocol.[57] The release of hemoglobin from erythrocytes was examined to investigate the interaction of polymers with cellular membranes. Therefore, human blood was collected in tubes with EDTA additive and was obtained from the Department of Transfusion Medicine of the University Hospital, Jena. The experiments were run in technical triplicates with blood from three blood donors. To remove the serum, the blood was centrifuged at 4500 × g for 5 min. After discarding the supernatant, the pellet of erythrocytes was washed three times with cold PBS (pH 7.4). The resulting suspension of erythrocytes was diluted 10-fold with PBS (pH 7.4). To aim for the polymer concentration of 10–150 µg mL^{-1}, the polymers were diluted with PBS (pH 7.4). Subsequently, 350 µL aliquots of erythrocyte suspension were added at the volume ratio of 1:1 to the polymer solutions. The erythrocyte-polymer suspensions were incubated at 37 °C and 5% (v/v) CO_2 atmosphere for 60 min. Afterward, the suspensions were centrifugated at 2400 × g for 5 min before the supernatant was transferred in triplicate to a transparent flat-bottomed 96-Fwell plate (VWR, Germany). The hemoglobin release was determined as the hemoglobin absorption at λ = 544 nm. Absorption at λ = 630 nm was used as a reference. Hundred percent hemolysis was achieved using 1% Triton X-100 as the positive control. Pure PBS was used as a negative control (0% hemolysis). The hemolytic activity of the polymer was calculated as follows:

$$\text{Hemolysis}/\% = \frac{(A_{\text{Sample}} - A_{\text{Negative control}})}{\left(A_{\text{Positive control}} - A_{\text{Negative control}}\right)} \cdot 100 \quad (6)$$

where A_{Sample}, $A_{\text{Negative control}}$, and $A_{\text{Positive control}}$ are the absorption values of a given sample, the PBS treatment, and the Triton X-100 treatment, respectively. A value less than 2% hemolysis rate was classified as non-hemolytic, 2 to 5% as slightly hemolytic, and values > 5% as hemolytic.

To determine the erythrocyte aggregation, a polymer solution was added as described above. Hundred microliters of the erythrocyte-polymer suspension was transferred to a transparent flat-bottomed 96-well plate (VWR, Germany) in triplicate. The cells were incubated at 37 °C, 5% (v/v) CO_2 atmosphere for 2 h, and the absorbance was measured at λ = 645 nm. Cells treated with PBS were the negative control, and cells treated with 50 µg mL^{-1} of 25 kDa LPEI were the positive control. The aggregation potential of the polymers was calculated as follows:

$$\text{Aggregation} = \frac{A_{\text{Negative control}}}{A_{\text{Sample}}} \quad (7)$$

where A_{Sample} and $A_{\text{Negative control}}$ are the absorption values of a given sample and the PBS treatment, respectively.

To determine the membrane-protecting effect of the polymers, additional investigation with hexadecyltrimethylammonium bromide (CTAB) was performed. Therefore, 350 µL isolated erythrocytes were incubated with 350 µL polymer dilutions for 10 min before 30 µg mL^{-1} of CTAB was added. The erythrocyte-polymer-CTAB suspensions were incubated at 37 °C and 5% (v/v) CO_2 atmosphere for 60 min before further centrifugation steps were performed. The hemoglobin release was measured, and the hemolytic activity was quantified. The study and experimental protocols used therein were approved by the ethics committee of the Jena University Hospital (2021-2058-Material).

Statistical Analysis: The statistical analyses were performed with Origin 8.2 Pro or OriginPro2022b software (Origin Lab, USA). A two-sample *t*-test with equal variance was applied to determine the statistical significance. All statistical significance was notated as $^{*}p \leq 0.05$, $^{**}p \leq 0.01$, and $^{***}p < 0.001$.

Supporting Information

Supporting Information is available from the Wiley Online Library or from the author.

Acknowledgements

L.S. and L.S.R. contributed equally as first authorship to this work. The authors gratefully acknowledge the Bundesministerium für Bildung und Forschung (BMBF, Germany, #13XP5034A PolyBioMik), the DFG Projects PolyTarget (SFB 1278, project B01, A05, C06, Z01, project ID: 316213987), Emmy-Noether Programme (Project-ID: 358263073), Heisenberg Programme (Project -ID: 514006196) as well as French National Research Agency (ANR- 20-CE09-0011-01). The authors further acknowledge the support by the "Thüringer Aufbaubank (TAB)" (2021 FGI 0005) and the "Europäischer Fond für regionale Entwicklung (EFRE)" (2018FGI0025) for funding of flow cytometry devices at the Jena Center for Soft Matter (JCSM). This research was further funded by the Hubert Curien Partnership (Campus France) and DAAD (German Academic Exchange Service, project number: 57604510) program PROCOPE 2022 allowing the mobility of Dr. Laurianne Simon to work at the JCSM. The authors thankfully acknowledge Carolin Kellner and Sandra Henk for taking care of the cell culture, Elisabeth Moek for her support in the uptake study, and Dr. David Pretzel for his support in imaging with LSM. The authors also warmly thank Paul Marque from the Organic Polymer Chemistry Laboratory of Bordeaux for the SLS analysis. Figures were created by BioRender.com.

Open access funding enabled and organized by Projekt DEAL.

Conflict of Interest

The authors declare no conflict of interest.

Data Availability Statement

The data that support the findings of this study are available from the corresponding author upon reasonable request.

Keywords

cholesterol, fast uptake, intracellular drug delivery, lipopolyoxazoline, membrane protection, poly(2-methyl-2-oxazoline)

Received: March 28, 2024
Revised: August 1, 2024
Published online: October 7, 2024

[1] B. Ghosh, S. Biswas, *J. Controlled Release* **2021**, *332*, 127.
[2] M. Ghezzi, S. Pescina, C. Padula, P. Santi, E. Del Favero, L. Cantù, S. Nicoli, *J. Controlled Release* **2021**, *332*, 312
[3] Z. Varanaraja, J. Kim, C. R. Becer, *Eur. Polym. J.* **2021**, *147*, 110299.
[4] K. Knop, R. Hoogenboom, D. Fischer, U. S. Schubert, *Angew. Chem.* **2010**, *49*, 6288.
[5] R. P. Garay, R. El-Gewely, J. K. Armstrong, G. Garratty, P. Richette, *Expert Opin. Drug Deliv.* **2012**, *9*, 1319.
[6] A. Moreno, G. A. Pitoc, N. J. Ganson, J. M. Layzer, M. S. Hershfield, A. F. Tarantal, B. A. Sullenger, *Cell Chem. Biol.* **2019**, *26*, 634.
[7] M. Mohamed, A. S. Abu Lila, T. Shimizu, E. Alaaeldin, A. Hussein, H. A. Sarhan, J. Szebeni, T. Ishida, *Sci. Technol. Adv. Mater.* **2019**, *20*, 710.
[8] Y. Ju, J. M. Carreño, V. Simon, K. Dawson, F. Krammer, S. J. Kent, *Nat. Rev. Immunol.* **2023**, *23*, 135.
[9] M. F. S. Deuker, V. Mailänder, S. Morsbach, K. Landfester, *Nanoscale Horiz.* **2023**, *8*, 1377.
[10] Y. Bavli, B.-M. Chen, G. Gross, A. Hershko, K. Turjeman, S. Roffler, Y. Barenholz, *J. Controlled Release* **2023**, *354*, 316.
[11] Y. Fang, J. Xue, S. Gao, A. Lu, D. Yang, H. Jiang, Y. He, K. Shi, *Drug Deliv.* **2017**, *24*, 22.
[12] X. Yao, C. Qi, C. Sun, F. Huo, X. Jiang, *Nano Today* **2023**, *48*, 101738.
[13] R. Luxenhofer, Y. Han, A. Schulz, J. Tong, Z. He, A. V Kabanov, R. Jordan, *Macromol. Rapid Commun.* **2012**, *33*, 1613.
[14] T. R. Dargaville, J.-R. Park, R. Hoogenboom, *Macromol. Biosci.* **2018**, *18*, 1800070.
[15] S. Nemati Mahand, S. Aliakbarzadeh, A. Moghaddam, A. Salehi Moghaddam, B. Kruppke, M. Nasrollahzadeh, H. A. Khonakdar, *Eur. Polym. J.* **2022**, *178*, 111484.
[16] T. Lorson, M. M. Lübtow, E. Wegener, M. S. Haider, S. Borova, D. Nahm, R. Jordan, M. Sokolski-Papkov, A. V Kabanov, R. Luxenhofer, *Biomaterials* **2018**, *178*, 204.
[17] G. Delaittre, *Eur. Polym. J.* **2019**, *121*, 109281.
[18] B. Guillerm, S. Monge, V. Lapinte, J.-J. Robin, *Macromol. Rapid Commun.* **2012**, *33*, 1600.
[19] K. Lava, B. Verbraeken, R. Hoogenboom, *Eur. Polym. J.* **2015**, *65*, 98.
[20] L. Simon, N. Marcotte, J. M. Devoisselle, S. Begu, V. Lapinte, *Int J Pharm.* **2020**, *585*, 119536.
[21] M. Rovira-Bru, D. H. Thompson, I. Szleifer, *Biophys. J.* **2002**, *83*, 2419.
[22] S. Zalipsky, C. B. Hansen, J. M. Oaks, T. M. Allen, *J. Pharm. Sci.* **1996**, *85*, 133.
[23] L. Simon, M. De Taddeo, A. Coeurvolan, M. Colpaert, J. Richard, J. M. Devoisselle, M. Morille, N. Marcotte, S. Bégu, V. Lapinte, *Int. J. Pharm.* **2023**, *642*, 123103.
[24] L. Simon, E. Bellard, B. Jouanmiqueou, V. Lapinte, N. Marcotte, J. M. Devoisselle, C. Lamaze, M. P. Rols, M. Golzio, S. Bégu, *Eur. J. Pharm. Biopharm.* **2022**, *180*, 308.
[25] S. Moein Moghimi, I. Hamad, T. L. Andresen, K. Jørgensen, J. Szebeni, S. Moein Moghimi, I. Hamad, T. L. Andresen, K. Jørgensen, J. Szebeni, *FASEB J.* **2006**, *20*, 2591.
[26] F. Ercole, M. R. Whittaker, J. F. Quinn, T. P. Davis, *Biomacromolecules* **2015**, *16*, 1886.
[27] P. Misiak, K. H. Markiewicz, D. Szymczuk, A. Z. Wilczewska, *Polymers* **2020**, *12*, 2620.
[28] Y. Zhou, V. A. Briand, N. Sharma, S. Ahn, R. M. Kasi, *Materials* **2009**, *2*, 636.
[29] Z.-Y. He, B.-Y. Chu, X.-W. Wei, J. Li, C. K. Edwards, X.-R. Song, G. He, Y.-M. Xie, Y.-Q. Wei, Z.-Y. Qian, *Int. J. Pharm.* **2014**, *469*, 168.
[30] H. Xu, M. Hu, X. Yu, Y. Li, Y. Fu, X. Zhou, D. Zhang, J. Li, *Eur. J. Pharm. Biopharm.* **2015**, *91*, 66.
[31] H. Xu, W. Zhang, Y. Li, F. F. Ye, P. P. Yin, X. Yu, M. N. Hu, Y. S. Fu, C. Wang, D. J. Shang, *Pharm. Res.* **2014**, *31*, 3038.
[32] I. Cazin, E. Rossegger, G. de la Cruz, T. Griesser, S. Schlögl, *Polymers (Basel)* **2021**, *13*, 56.

[33] A. Féron, S. Catrouillet, S. Sene, G. Félix, B. T. Benkhaled, V. Lapinte, Y. Guari, J. Larionova, *Nanomaterials* **2024**, *14*, 906.
[34] L. Korchia, C. Bouilhac, J.-J. Robin, V. Lapinte, *Eur. Polym. J.* **2017**, *88*, 636.
[35] M. Danaei, M. Dehghankhold, S. Ataei, F. Hasanzadeh Davarani, R. Javanmard, A. Dokhani, S. Khorasani, M. Mozafari, *Pharmaceutics* **2018**, *10*, 57.
[36] M. Stemmelen, C. Travelet, V. Lapinte, R. Borsali, J.-J. Robin, *Polym. Chem.* **2013**, *4*, 1445.
[37] X. Zhang, P. Tanner, A. Graff, C. G. Palivan, W. Meier, *J. Polym. Sci. A* **2012**, *50*, 2293.
[38] H.-R. Jia, Y.-X. Zhu, K.-F. Xu, X. Liu, F.-G. Wu, *J. Controlled Release* **2018**, *286*, 103.
[39] A. Oudin, J. Chauvin, L. Gibot, M.-P. Rols, S. Balor, D. Goudounèche, B. Payré, B. Lonetti, P. Vicendo, A.-F. Mingotaud, V. Lapinte, *J. Mater. Chem. B* **2019**, *7*, 4973.
[40] L. Simon, M. De Taddeo, A. Coeurvolan, M. Colpaert, J. Richard, J. M. Devoisselle, M. Morille, N. Marcotte, S. Bégu, V. Lapinte, *Int. J. Pharm.* **2023**, 123103.
[41] A. Rawat, A. Vijaya Bhaskar Reddy, *Eur. J. Med. Chem. Rep.* **2022**, *5*, 100038.
[42] I. V. Zhigaltsev, P. R. Cullis, *Langmuir* **2023**, *39*, 3185.
[43] F. Hullin-Matsuda, R. Ishitsuka, M. Takahashi, T. Kobayashi, in *Lipidomics*, Humana Press, Totowa, NJ **2009**, p. 203.
[44] J. J. Rennick, A. P. R. Johnston, R. G. Parton, *Nat. Nanotechnol.* **2021**, *16*, 266.
[45] D. Vercauteren, R. E. Vandenbroucke, A. T. Jones, J. Rejman, J. Demeester, S. C. De Smedt, N. N. Sanders, K. Braeckmans, *Mol. Ther.* **2010**, *18*, 561.
[46] G. Griffiths, J. Gruenberg, M. Marsh, J. Wohlmann, A. T. Jones, R. G. Parton, *Adv. Drug Delivery Rev.* **2022**, *188*, 114403.
[47] H.-J. Chen, Y.-A. Cheng, Y.-T. Chen, C.-C. Li, B.-C. Huang, S.-T. Hong, I.-J. Chen, K.-W. Ho, C.-Y. Chen, F.-M. Chen, J.-Y. Wang, S. R. Roffler, T.-L. Cheng, D.-H. Wu, *Cancer Nanotechnol.* **2023**, *14*, 78.
[48] Y.-C. Su, P.-A. Burnouf, K.-H. Chuang, B.-M. Chen, T.-L. Cheng, S. R. Roffler, *Nat. Commun.* **2017**, *8*, 15507.
[49] R. Luxenhofer, G. Sahay, A. Schulz, D. Alakhova, T. K. Bronich, R. Jordan, A. V. Kabanov, *J. Controlled Release* **2011**, *153*, 73.
[50] P. Misiak, K. Niemirowicz-Laskowska, K. H. Markiewicz, I. Misztalewska-Turkowicz, P. Wielgat, I. Kurowska, G. Siemiaszko, M. Destarac, H. Car, A. Z. Wilczewska, *Int. J. Nanomed.* **2020**, *15*, 7263.
[51] H.-Y. Wang, X.-W. Hua, H.-R. Jia, P. Liu, N. Gu, Z. Chen, F.-G. Wu, *J. Mater. Chem. B* **2016**, *4*, 834.
[52] S. Sevimli, S. Sagnella, A. Macmillan, R. Whan, M. Kavallaris, V. Bulmus, T. P. Davis, *Biomater. Sci.* **2015**, *3*, 323.
[53] Y. S. Lai, Y. Zhou, E. Eustance, L. Straka, Z. Wang, B. E. Rittmann, *Algal. Res.* **2018**, *34*, 250.
[54] S. Raisin, M. Morille, C. Bony, D. Noël, J.-M. Devoisselle, E. Belamie, *Biomater. Sci.* **2017**, *5*, 1910.
[55] I. Passagne, M. Morille, M. Rousset, I. Pujalté, B. L'Azou, *Toxicology* **2012**, *299*, 112.
[56] S. Le Saux, H. Aarrass, J. Lai-Kee-Him, P. Bron, J. Armengaud, G. Miotello, J. Bertrand-Michel, E. Dubois, S. George, O. Faklaris, J.-M. Devoisselle, P. Legrand, J. Chopineau, M. Morille, *Biomaterials* **2020**, *231*, 119675.
[57] F. Richter, L. Martin, K. Leer, E. Moek, F. Hausig, J. C. Brendel, A. Traeger, *J. Mater. Chem. B* **2020**, *8*, 5026.